Development of a MEMS based dynamic rheometer†

Gordon F. Christopher,*[a] Jae Myung Yoo,[b] Nicholas Dagalakis,[b] Steven D. Hudson*[a] and Kalman B. Migler*[a]

Rheological methods that interrogate nanolitre scale volumes of fluids and solids have advanced considerably over the past decade, yet there remains a need for methods that probe the frequency-dependent complex rheological moduli through application of homogenous strain fields. Here we describe a Micro-Electro-Mechanical System (MEMS) based approach for the measurement of dynamic rheology of soft matter where oscillatory strain is produced in a sample sandwiched between an oscillating MEMS stage and a glass plate. The resulting stress–strain relationships are revealed by measurement and analysis of the stage motion. We present preliminary data on simple viscous fluids and on viscoelastic thin films. In this proof-of-principle device, we measure moduli in the range of 50 Pa to 10 kPa over a range of 3 rad s^{-1} to 3000 rad s^{-1} using less than 5 nL of sample material. The device's measurement window is limited primarily by our current ability to measure the motion of the stage. This device will provide a new way to characterize dynamic microrheology of an array of novel materials and will prove useful in a number of areas including biorheology, microfluidics and polymer thin films.

Introduction

The dynamic response of complex fluids and soft matter to flow and deformation has industrial applications in cosmetics, food, medicine and other fields. Complex fluids and soft matter contain microcomponents such as dissolved polymers, suspended colloids, or emulsion drops which give rise to a microstructure larger than the individual components. This microstructure imparts viscoelastic and viscoplastic behavior to the material.[1,2] In recent years, the ability to create flow cells smaller than 100 μm in diameter for processing these materials has introduced confinement and deformation on the same length scale as the microstructure and increased interaction between solid boundaries and the fluid.[3] Since the non-Newtonian behavior of these materials derives from the microstructure deformation, confinement on the same length scale as the microstructure should affect their flow behavior.[1–6]

In addition to confinement effects, the use of novel and experimental materials often results in a paucity of sample to characterize. Rheology is an important tool in material characterization. Nonetheless, traditional rheometers need multiple millilitres of material for testing. In a traditional dynamic rheometer, the fluid is subject to an oscillatory shear field and the viscoelastic moduli are extracted over a range of test frequencies. The growing need to understand the rheology of small sample volumes or confined soft matter has lead to an increasing interest in microrheology, which uses smaller sample volumes than traditional techniques. Microrheology can be broadly defined as experimental methods that measure the rheology of fluids and

materials at length scales from 0.5 μm to 100 μm. However, there are no microrheology methods that are directly analogous to the dynamic rheometer.

We propose and test a proof-of-principle dynamic rheometer which operates at the microscale via MEMS technology. It is able to confine materials down to 1 μm with deformation on the same length scale using less than 5 nL of material. The MEMS oscillatory shear microrheometer (MEMS-μR) measures both storage and loss modulus over a range of frequencies. The MEMS-μR strains the whole fluid body, so that the entire microstructure response to deformation is characterized, addressing a current gap in microrheology.

Background

The broad classes of existing microrheology methods include steady state flows, thin film rheology and oscillatory microrheology.[2,3,6–8] Using microfluidics or a microgap rheometer, steady shear rates or strains can be applied to a sample material, and a steady state viscosity can be measured. Microfluidic geometries can be used to confine complex fluids and characterize materials' viscosities through measurement of flow rates, pressure drops, and flow visualization. Microfluidic geometries such as capillaries, stagnation flows, and contractions have all been used to measure viscosity as a function of shear rate for complex fluids including dilute polymer solutions, rod like molecule solutions, wormlike micelle solutions[3] and polymer melts.[9] A potential problem with some microfluidic methods is that although nominally planar, confinement creates a more 3-dimensional flow than in macrofluidics.[10,11] Steady state responses of complex fluids under confinement have also been characterized using the Flexure Based Microgap Rheometer (FMR). The FMR uses a series of macroflexures to apply a steady linear strain to a sample confined down to approximately 100 nm. By controlling shear rate and measuring stress, the FMR can extract viscosity, and has been used to study the

[a]Complex Fluids Group, Polymers Division, NIST, Gaithersburg, MD, 20899, USA. E-mail: gchris@nist.gov; kmigler@nist.gov; shudson@nist.gov
[b]Systems Integration Group, Intelligent Systems Division, NIST, Gaithersburg, MD, 20899, USA
† Official contribution of the National Institute of Standards and Technology, not subject to copyright in the United States.

effects of confinement on viscosity, yield stress and slip in a number of systems.[4,5]

Due to the growing industrial use of thin films, the rheology of films with thicknesses less than 1 μm has also been extensively studied. Techniques including thin film buckling[12] and nano-indentation[7] have been developed to deform the materials at the microlength scale. Thin film buckling uses compressive strain to create wrinkles in a film, which are a function of the film's thickness and elastic modulus. The temporal response to the buckling yields the stress relaxation modulus of the film. It has been used with success to characterize a number of systems.[12–15] Nanoindentation uses a microprobe to deform a surface, measuring the loading on the probe to extract elastic moduli.[7] Factors that affect this technique include probe dimension, film thickness, substrate material, system stiffness, contact area, and the constitutive equations used to model material properties. Although it is possible to use nanoindentation to extract visco-elastic properties,[8,16–19] the effects of adhesion, system compliance, and complex analysis make measurement of viscoelastic materials difficult.[7,8,12,18]

In order to measure dynamic microrheology, particle tracing is a widely used method. Particle tracing microrheology is a broad term referring to any technique that uses the motion of particles in a complex fluid to extract relevant rheological properties.[20] Initially particle tracing microrheology was done using scattering based techniques, such as diffusing wave spectroscopy, to measure the displacement of many particles in a sample volume.[21] A subset of this technique is particle tracking micro-rheology, which examines the motion of a single particle through optical or other methods.[6,22] Passive particle tracing micro-rheology measures the displacement of tracer particles through a sample material due to thermal diffusion and then uses the generalized Stokes–Einstein equation to extract complex viscosity.[6] Active particle tracing microrheology uses external fields to move particles through an applied force.[23–25] The force on the particles and their displacement are used to measure the storage and loss modulus of the surrounding sample.[2] These techniques have shown agreement with bulk rheology

measurements and use much smaller sample sizes than traditional bulk methods. The probe particle can significantly affect results through interaction with the surrounding medium, so appropriate selection of the particles is necessary to obtain accurate results. Particle tracing microrheology measures local properties—those in the immediate vicinity of the particle—which may be different from the overall properties of the fluid. Also, although deformation is on the same length scale as the microstructure, there is generally no confinement without using additional techniques like microfluidics.[2,6] In order to extract dynamic microrheology with confinement, MEMS based oscillatory squeeze flow rheometers that extensionally strain an entire fluid body with confinement of approximately 100 μm have been theorized[26,27] and developed.[28] This technique is sensitive to interfacial tension and surface rheology, due to deformation of the air/liquid surface, and uses volumes of fluid up to 100 μL.

MEMS approach

In order to create a microrheometer that deforms an entire fluid structure and measures both storage and loss moduli using minimal fluid volumes, a MEMS based 1D nanopositioner stage (Fig. 1) is used to apply a linear strain to a sample material. The test fluid (or film) is placed between the stage and an upper fixed plate (gap height, h). Using this device, a sample material can be deformed up to 1000% strain, depending on the gap height. As shown in schematic on the right side of Fig. 1, the final config-uration of stage, fluid, and fixed plate creates a linear parallel plate rheometer. The details of the MEMS device and the methodology by which we measure viscoelastic moduli are described below.

MEMS 1D nanopositioner stage

Our measurement platform is based on a planar MEMS device. Actuation of the MEMS stage creates an oscillatory flow in the sample, while its finite compliance creates the means by which the moduli are measured. The left side of Fig. 1 shows a single crystal
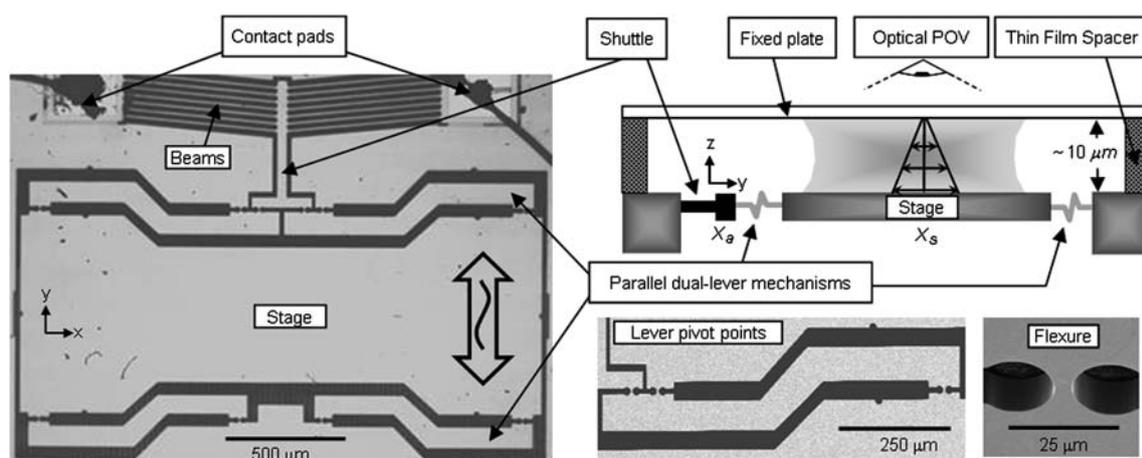

Fig. 1 (Left) Reflected light optical micrograph of a MEMS 1D nanopostioner used to create a MEMS oscillatory shear microrheometer (MEMS-μR). (Right top) Conceptual schematic (not to scale) of MEMS-μR. Both stage and levers are approximately 20 μm thick and suspended at the top surface of a 300 μm wafer. (Right bottom) SEM image of the lever that amplifies actuator motion and drives stage. Tilted close-up image of the circular flexures which connect levers to stage and wafer.

silicon MEMS Parallel Dual Lever-NanoPositioner (PDL-NP), featuring two parallel sets of lever beams which pivot on flexures. These parallel levers keep the dog-bone shaped stage, which has maximum dimensions of 2.04 mm × 0.82 mm × 20 μm, suspended at the top of the silicon wafer. The stage is driven by a thermal bent-beam actuator which works by applying an alternating current between the two contact pads connected to the chevron arrangement of suspended beams in parallel. Joule heating causes the beams to expand and then buckle. Due to their physical constraints, the buckling causes a linear motion at the apex of the chevron.[29] The thermal actuator is used because it requires low voltage input (10 V), but it operates at a lower bandwidth and generates more heat than an electrostatic actuator would.[30] Due to the nature of the actuator, we note that the frequency of the actuator motion is actually double that of the applied voltage. (When referring to the driving frequency throughout this article, we mean the frequency of the actuator rather than that of the applied voltage.) The device's resonant frequency is approximately 38 000 rad s⁻¹, while the first order system bandwidth, the point at which the stage's amplitude reduces by 3 dB, is (500 ± 100) rad s⁻¹.[31] Since we operate below and above this latter frequency, the unloaded stage amplitude is measured at each frequency tested. The mechanisms were fabricated on site using standard MEMS fabrication techniques.

The input displacement is generated by the thermal actuator and transmitted to the levers through small flexures (Fig. 1). These levers pivot about another set of flexures, transmitting the actuator force to the moving stage through a final set of flexures at the opposite end of the lever. Because these flexures operate symmetrically on a rigid body, they experience balanced elastic deformation, resulting in the virtual cancellation of parasitic cross-axis motion.[32] A second set of levers similarly constrains the other end of this stage providing structural support. The symmetric mechanical design results in a linear motion parallel to the y axis with a maximum displacement of approximately 12 μm.[31] Finite element modeling of the PDL-NP predicts a spring stiffness of 37.5 N m⁻¹ for each individual lever, which results in an effective spring constant, k_s, of 75 N m⁻¹ for the double lever system, which is consistent with measurements performed using an Atomic Force Microscope (AFM). Using the known mass of the stage (0.102 μg), this spring constant predicts a resonance frequency of 38 315 rad s⁻¹, which is the resonant frequency observed experimentally.

Methodology

The MEMS-μR does not measure the response stress due to the applied strain. Instead, the dynamics of the moving stage are used to obtain moduli. A given applied voltage and frequency will move the unloaded stage in phase with the actuator at a fixed amplitude. When the sample is loaded, it resists the stage motion. This resistance force will decrease the amplitude of the stage motion and cause it to move out of phase with the actuator (Fig. 2a). Using measurements of the amplitude and the phase angle of the loaded stage, the dynamic moduli at an applied frequency are obtained.

The experiments are carried out using a reflected light microscope with either 50× (NA = 0.75) or 100× (NA = 0.90) objectives. The motion of the stages is captured using a high
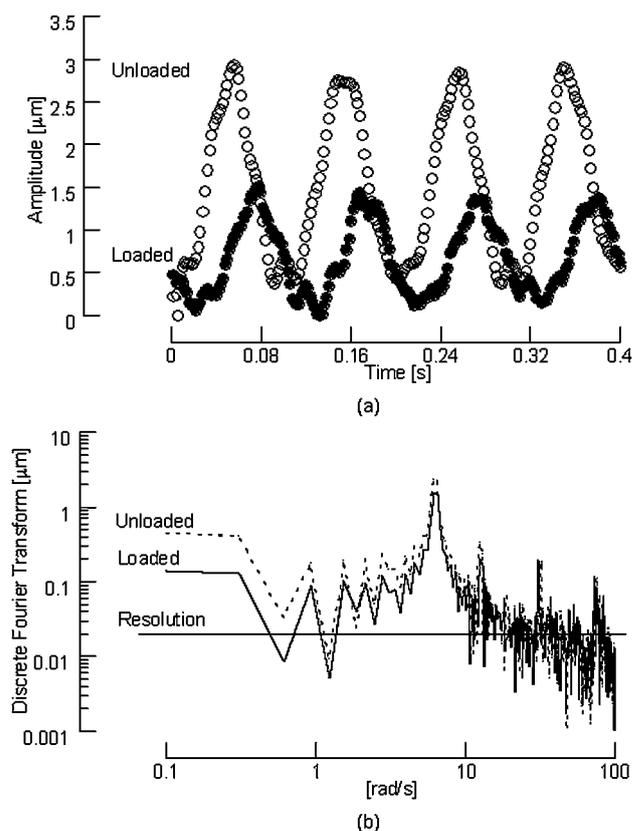

Fig. 2 (a) Stage motion of MEMS-μR being driven at 62.8 rad s⁻¹ both unloaded and loaded with 2 Pa s silicone oil. The loaded response displays a reduction in amplitude due to viscous forces acting on the stage. The relative phase of these signals is referenced to the actuator. (b) Fast Fourier transform of stage motion data. Both unloaded and loaded devices display peaks at the driving frequency and other harmonics.

speed camera (Redlake, HG 100K)‡ capable of frame rates up to 15 000 fps. For a given driving frequency the camera is set such that the frame rate is 100 times greater than the driving frequency and at least 10 cycles of motion are recorded. The camera is focused on the edge of the stage across from the actuator shuttle, allowing a single movie to capture the stage amplitude and its phase difference from the actuator.

Since our analysis method relies on comparison of the loaded and unloaded motion of the stage, the motion of the unloaded MEMS stage for a fixed number of frequencies is tested first. Although the dynamics of every stage are ideally identical, small differences in each stage's dynamic response could affect results. Examination of our data shows that at a given frequency, stage to stage variation of the unloaded amplitude is ±6%. This variation can be attributed to slightly different spring constants in the PDL-NP flexures and variation in the thermal actuators. The uncertainty caused by variation in the spring constants (as observed by variations in the unloaded amplitudes) is not

‡ Certain commercial products and processes are identified in this article to foster understanding. Such identification does not imply recommendation or endorsement by the National Institute of Standards and Technology, nor does it imply that the products and processes identified are necessarily the best available for the purpose.

factored into the analysis as other experimental uncertainties (see below) are typically more significant.

For testing viscous fluids, the rheometer is loaded and then run through the same experimental conditions as the unloaded stage. The stage is loaded with approximately 5 nL of a sample fluid using a 0.5 µL syringe (SGE Analytical Science, H02-A1270) and a syringe pump for small volume syringes (KDS 310 Syringe Pump). Based on manufacturer specifications, the pumps are accurate to ±0.2 nL for a 5 nL drop. When transferring the drop to the stage we do not remove all of the liquid from the syringe tip. Based on measurements of the fluid area, A_0, and the height of the gap, we are able to place approximately 50% to 75% of the volume onto the stage. A transparent coverslip is used as the fixed plate above the stage. The gap between the 2 plates is set with a polymer thin film of fully cross-linked PDMS (Sylgard 184) that is spun onto the coverslip to create the desired thicknesses of 1 µm to 10 µm.[33,34] The film thickness is measured with white light interferometry and the films exhibit uniformity of ±0.2 µm.§ The thin film is removed from a portion of the coverslip, and this section is placed over the stage to accommodate the sample fluid completing the rheometer. A single stage can only be used to test one sample through a range of frequencies because once loaded, attempts to unload the stage generally damage it. Although each device is single use, cost per finalized device is reduced due to the batch nature of MEMS fabrication techniques resulting in tens to hundreds of individual devices per single silicon wafer.

For analysis purposes, the film thickness is used for the height of the gap, h, in the final analysis. We do expect that surface tension will deflect the stage upward, shrinking the gap somewhat. In order to estimate this effect, the upward force caused by the surface tension can be balanced with the out of plane spring force of the stage. Modeling of the stage suggests that the out of plane spring stiffness is 65 N m^{-1}, and the value is consistent with tests performed using an Atomic Force Microscope. Assuming a surface tension of 21 mN m^{-1} for an oil/air interface,[35] we estimate that the stage will deflect approximately 0.48 µm. We did not measure the actual deflection of the stage, and rely on the measured film thicknesses in all subsequent analysis.

The testing of a viscoelastic thin film requires a different loading procedure. The sample material is spun onto a coverslip to a desired thickness. The coverslip with the spun film is placed over the stage. The film must make conformal contact with and adhere to the stage, or the stage will slip on the film surface. The film may also make conformal contact with the back levers holding up the stage. This should not greatly affect the results since this area of contact is much smaller than that of the entire stage. This contact may cause the film to delaminate from the stage because the stress in the film at stage's edge and at the lever will differ. Since the thin films tested are approximately 5 µm thick and the space between the levers and the stage is 50 µm, delamination is not a concern. With both fluid samples and thin films, the weight of the glass and the adhesion of the film to the substrate surrounding the PDL-NP anchor the top plate to the substrate.

Image processing and analysis takes place after experimentation. To extract the motion of the stage, a custom programmed

§ Reported data point uncertainties represent one standard deviation or propagation of uncertainty based on one standard deviation of fitted values.
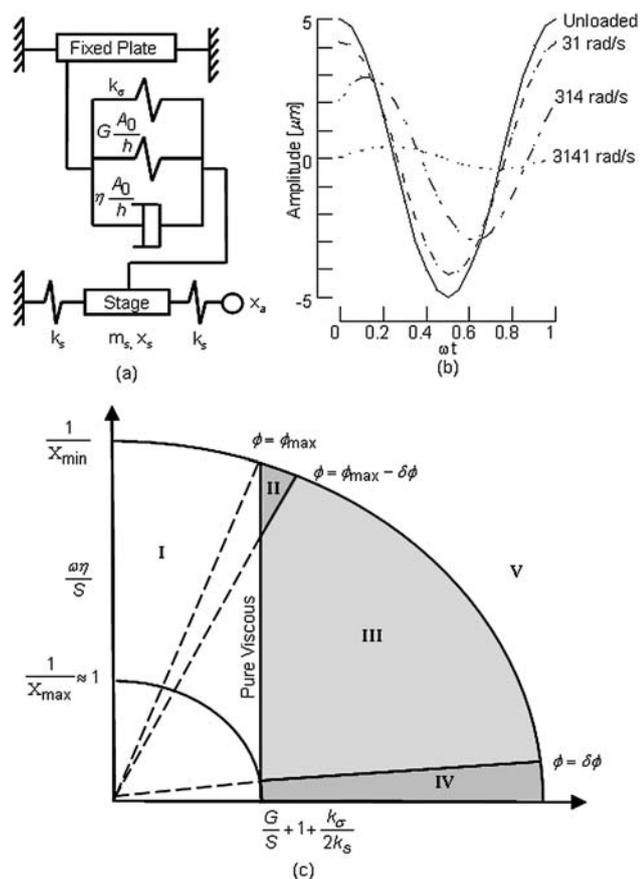
routine is used. An edge detection algorithm analyzes the gray-scale image to locate the edge of the stage and track its movement.[36] By using this edge detection method, we are able to obtain sub-pixel resolution of the stage position with uncertainty of ±0.08 pixels (±17 nm). We can clearly resolve the motion of a damped stage, capturing approximately 50 points per cycle, even as the amplitude decreases to 0.75 µm (Fig. 2a). Although our spatial resolution is high, it should be possible to improve both our spatial and temporal resolution in the future by using a different detection method, such as a laser and photodiode system, which should improve device accuracy.

Once the raw movies have been processed, sine curves are fit to the data. In the case of the unloaded data, we note through fast Fourier transform that although the driving frequency is the dominant response, higher order harmonics are also observed. We also note a low frequency response at approximately 0.01 rad s^{-1} due to room and instrument vibration. These frequencies are observed in the loaded stages as well. These other modes typically represent less than 10% of the amplitude power spectrum of the resultant stage motion (Fig. 2b). To ensure an accurate representation of the data, the stage motion is fit to a summation of 4 modes.

$$x_s = \sum_{i=1}^{4} x_i \sin(\omega_i t + \phi_i) \tag{1}$$

Only the driving frequency response is used in the analysis of the fluid properties. In order to find the stage's phase angle, the actuator motion is also fit to a series of sine curves, and the difference in phase between the stage and the actuator is used. Once the primary amplitudes and phase angles are obtained from the curve fits, they are used with the model described below to obtain the storage modulus and viscosity/loss modulus for a given frequency.

Using this methodology, the rheometer is neither stress nor strain controlled. We simply set a voltage and frequency and let the system respond naturally to the applied actuation. We then use the model to extract the relevant rheological data. In the future, we could adjust our methodology by using real-time analysis to actively measure the strain and use the model to calculate the stress. Using a feedback control loop, we could then operate the MEMS-µR in either stress or strain controlled modes by adjusting the applied voltage.

Model

In order to use the MEMS-µR to characterize a material, the motion of the loaded stage is used to ascertain the viscous and elastic shear forces, which are then used to extract loss and storage moduli. To accomplish this, the forces acting on the stage are modeled using a mechanical analog (Fig. 3a). The stage is modeled as a mass, m_s, suspended between two springs with stiffness, k_s. The effective motion of the thermal actuator due to the mechanical advantage of the levers is x_a, and the stage motion is x_s. The mass of the fluid is ignored since it is much smaller than the mass of the stage. The sample material is modeled as a Voigt element, which represents a linear viscoelastic material as a spring and a dashpot in parallel with stiffness defined by shear modulus, G, and viscosity, η, respectively. The Voigt element has only a single

Fig. 3 (a) Mechanical representation of MEMS-µR with fluid modeled as a Voigt element. (b) Model prediction of MEMS-µR response to increasing frequency for a 10 Pa s oil. Both amplitude and phase angle are affected. (c) Representation of phase space converting measured amplitude, X, and phase angle, ϕ, to relevant rheological parameters viscosity, η, and storage modulus, G. Region I is to the left of the pure viscous response line and is physically inaccessible. In region II, loss moduli only can be measured due to phase angle resolution. Region III is the theoretical measurement window where both loss and storage moduli can be measured. In region IV, storage moduli only can be measured due to phase angle resolution. Region V is to the right of the $1/X_{min}$ arc and cannot be measured due to amplitude resolution.

relaxation time and assumes a uniform strain loading in the fluid. For linear viscoelastic behavior, input and output frequencies are the same and the single element is therefore sufficient to model the fluid response.[37] An additional spring is added to the Voigt element, to represent the effects of the surface tension on the moving stage, with a representative stiffness, k_σ. If we assume small angle deformation, θ, which should be valid for strains less than 10%, the spring constant can be estimated by characterizing the force due to surface tension as follows:

$$F_\sigma = 4r\sigma \times \sin(\theta) = \frac{4r\sigma}{h}x_s \quad (2)$$

$$k_\sigma = \frac{4r\sigma}{h} \quad (3)$$

Here we assume that the area of contact is a circle with radius, r, and that the magnitude of the surface tension force is the

perimeter of that circle projected onto the direction of motion times the surface tension, σ. We assume that the net force is the sine of the angle caused by the displacement of the stage. Using eqn (3), we can estimate that the surface tension stiffness due to the silicone oils is approximately 15 N m⁻¹, which is slightly less than about half of the combined effect of the 2 pairs of parallel levers in series, $0.5k_s = 37.5$ N m⁻¹. A force balance on the device results in the following dynamic equation for the motion of the stage.

$$\frac{m_s}{k_s}\ddot{x}_s + \frac{\eta(A_0/h)}{k_s}\dot{x}_s + \left(2 + \frac{G(A_0/h) + k_\sigma}{k_s}\right)x_s = x_a \quad (4)$$

Using eqn (4), we can predict both the amplitude and phase angle shift for a fluid of known properties over a range of frequencies (Fig. 3b). We remove the actuator amplitude by normalizing the response of the loaded stage by the unloaded stage amplitude, resulting in the following equation for the stage response:

$$\frac{x_{s,loaded}}{|x_{s,unloaded}|} = X\sin(\omega t + \phi) \quad (5)$$

Eqn (4) and (5) yield:

$$G\left(\frac{A_0}{h}\right) + k_\sigma + 2k_s - \omega^2 m_s = \left(\frac{2k_s - \omega^2 m_s}{X}\right)\cos(\phi) \quad (6)$$

$$\omega\eta\left(\frac{A_0}{h}\right) = \left(\frac{2k_s - \omega^2 m_s}{X}\right)\sin(\phi) \quad (7)$$

As the experiments are performed well below the resonance frequency, $\omega_r = (2k_s/m_s)^{1/2}$, we can simplify eqn (6) and (7) to:

$$\frac{G}{S} = \frac{\cos(\phi)}{X} - 1 - \frac{k_\sigma}{2k_s} \quad (8)$$

$$\frac{\omega\eta}{S} = \frac{\sin(\phi)}{X} \quad (9)$$

where $S = 2k_s h/A_0$ is termed the stage constant. The measured phase angle, ϕ, and normalized amplitude, X, can be used to compute the moduli as described in eqn (8) and (9) and shown graphically in Fig. 3c. The value of the stage constant sets the order of magnitude of the values of the moduli that can be measured with the MEMS-µR. The uncertainty and dynamic range of the measurements of ϕ and X determine the measurement window for G and η. The viscosity window is limited on the low end when the phase angle becomes too small to measure accurately by $S\delta\phi/\omega < \eta$ and on the high end when the normalized amplitude becomes too small to measure accurately by $\eta < S/\omega\delta x$, where δx and $\delta\phi$ are the respective uncertainties in X and ϕ. Using $S \approx 1000$ N m⁻² and measurement uncertainties $\delta x = 0.05$ and $\delta\phi = 0.1$ rad (which are the typical uncertainties on these values seen in experimental results), the theoretical measurement window is 100 Pa < $\eta\omega$ < 20 000 Pa. A similar consideration for G leads to a window of 50 Pa < G < 20 000 Pa as long as both k_s and k_σ are known (Fig. 3c).

While, the stage constant sets the measurable magnitude of the moduli, the measurement range is further limited by the phase

angle resolution, $\partial\phi$, similar to commercial oscillatory rheometers. Recalling that $\tan\phi \approx G''/G'$, the minimum resolution of the phase angle gives a measurement limit of $G''/G' > 0.1$. If the ratio of the moduli is not greater than this value, the loss modulus is below the sensitivity of the system and cannot be accurately resolved. The storage modulus can still be measured. For example, when the elastic modulus reaches the upper limit of the MEMS-µR (20 000 Pa), the lower sensitivity of the loss modulus will increase from 100 Pa to 2000 Pa (Fig. 3c).

For purely or dominantly viscous material, there is always some elasticity in the system due to the stage springs. For purely viscous materials, we observe that the response of the phase angle and normalized amplitude create a vertical line in the measurement window (Fig. 3c). Due to the maximum sensitivity of the system set by S, there is also a maximum phase angle measurable. Assuming the same values as earlier, this maximum phase angle is approximately 1.5 rad. There is a small region, 1.4 rad $< \phi$ < 1.5 rad, in which the lower limit of the measurable elastic modulus is increased from 50 Pa to 1000 Pa, because any changes in phase angle are below the resolvable limit. In this window, only the loss modulus is measured (Fig. 3c).

While surface tension is not relevant in the case of continous viscoelastic solid films, it must be carefully considered in viscoelastic liquids, which are circumscribed by a meniscus. We use the capillary number, Ca, to estimate the relative magnitude of the surface tension to the viscous shear force.

$$\mathrm{Ca} = \frac{x_{\mathrm{s,loaded}}\,\omega\eta r}{2h\sigma} \quad (10)$$

Fig. 4 shows the capillary number as a function of frequency for two different viscosity fluids. The model should be relatively insensitive to surface tension when Ca > 0.1. Below that value, extracting the viscosity and elasticity is difficult without *a priori* knowledge of the surface tension. We note that analysis of the stage motion at low frequencies could be used in the future to analyze the surface tension.

Similar to surface tension, it is the possible that surface rheology could affect the MEMS-µR for complex viscoelastic fluids (but not films). Nonetheless, this is true in general for most dynamic rheometers, since the sample aspect ratio is similar. A surface with a distinct viscoelastic rheology could add up to 4 additional elements (elastic and viscous moduli for both shear
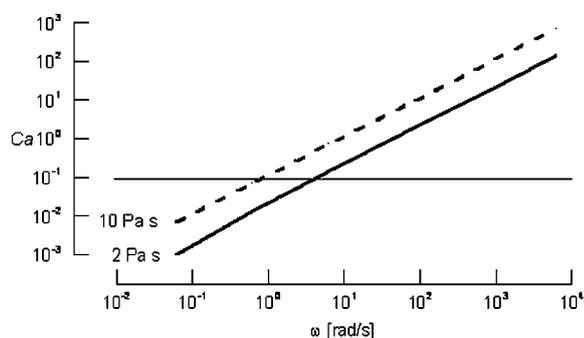
and dilatational modes of deformation) in parallel to the fluid's bulk properties in the mechanical analog model. Without *a priori* knowledge of the surface rheology, we are unable to distinguish its effect from the bulk's.

For surface shear deformation, the elastic force contribution would take the same form as eqn (3), and the surface modulus would replace surface tension. Typical moduli for viscoelastic surfaces can be as low as 10^{-9} N m^{-1} and up to 10^{-2} N m^{-1} for a protein laden interface. At the higher values, the effect of shear surface rheology would be similar to surface tension force. The dilatational deformation is more complex and is dependent on the square of the surface deformation. It is therefore less significant at small strains. If dealing with systems with relatively high bulk moduli values, these forces are safely ignored, but there are a number of materials where surface rheology can affect the results of the rheometer.

Materials

The MEMS-µR was tested using two viscous fluids and two viscoelastic films. The viscous fluids were a 10 Pa s silicone oil (Gelest) and a 2 Pa s mineral oil (Canon Instruments Viscosity Standard). Both of these materials wet the silicon wafer completely and have stable viscosities over a range of temperatures. The viscoelastic film was from PDMS (Sylgard 184). The commercial product is a 2 part elastomer, a base, A, and a cross-linking agent, B. The base is a Newtonian fluid nearly identical to the silicone oil used in the viscous calibration. The cross-linker concentration determines the number density of the cross-links and hence the elastic and viscous moduli. For the tests reported in this study, B : A ratios of 1 : 100 and 1 : 30 by mass were used to create thin films with varying properties (referred to as 1% and 3% PDMS). The films were spun to a thickness of 1 µm to 10 µm by first mixing the base in toluene and then the desired amount of cross-linking agent.[33,34] Films were cured overnight at 100 °C, and then removed and left at room temperature until testing began.

Viscosity standards

In order to test the viability of the MEMS-µR and accuracy of the proposed model, a series of initial tests on constant viscosity, non-elastic standard fluids was performed (*i.e.*, $G \equiv 0$ and $\eta =$ constant). We first tested the device with an air gap ($G = 0$ Pa and $\eta = 0$ Pa s) where the trivial limit of eqn (4) and (5) yields $X = 1$ and $\phi = 0$. Experimentally, we observe $\phi = (0.00 \pm 0.05)$ rad over a range of frequency from 3 rad s^{-1} to 3000 rad s^{-1}, consistent with our expectations. We next tested the device on the fluids of interest.

For the 2 Pa s oil, the model accurately predicts both the normalized amplitude, X, and the phase angle, ϕ, observed experimentally (Fig. 5). The normalized amplitude did not vary significantly until frequencies above approximately 60 rad s^{-1}, which is consistent with modeling (Fig. 5a). The strain on the sample is not constant and decreases from approximately 18% to 6%, which was typical for the viscous experiments (Fig. 5b). Because the unloaded and loaded amplitudes vary differently, the strain does not display the same functional form as X. The experimental phase angle and the predicted value display good
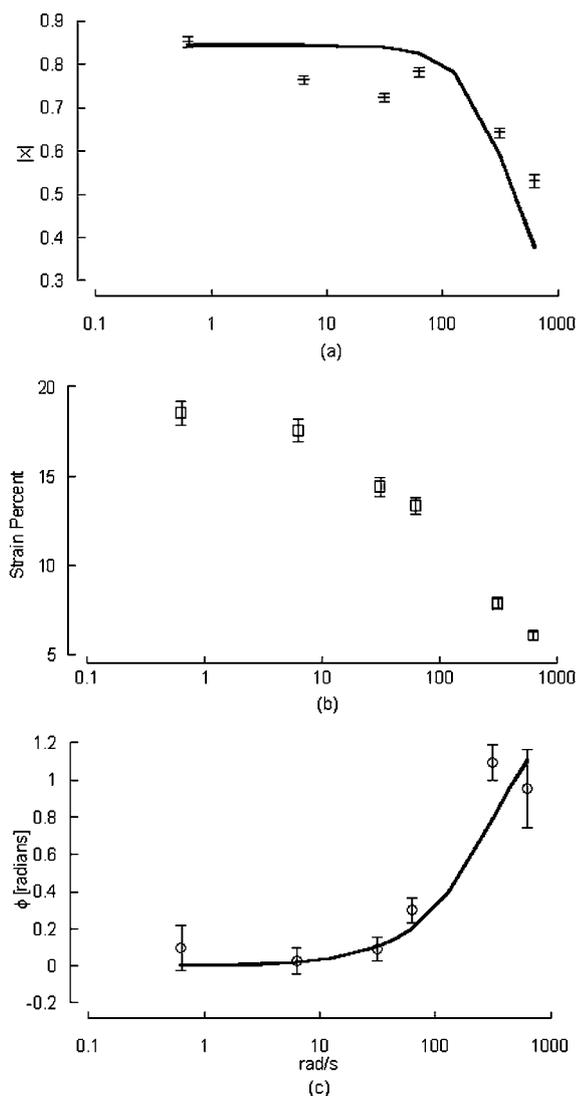

Fig. 4 Capillary number as a function of frequency for two different viscosity fluids, assuming 5 nL of fluid, a gap height of 5 µm, surface tension of 35 mN m^{-1} and a stage amplitude of 10 µm. Surface tension significantly affects the results when Ca $\ll$ 0.1.

Fig. 6 Viscosity results for 2 test viscosity standard fluids, 10 and 2 Pa s oils. Lines represent known values. Points at identical frequencies have been horizontally offset slightly to make graph clearer. Shaded area represents theoretical measurement window as described in the text.

majority of the uncertainty in the viscosity is due to the uncertainty on the small phase angles, $\delta\phi$, so increasing accuracy of this measurement will significantly improve overall accuracy. For all the frequencies shown, the average value of the elastic modulus is 50 Pa, which approaches the minimum resolution of the device and the expected value of 0.

The extracted viscosities approximate the known values. For the first generation device using optical microscopy, these results represent a confirmation of the proof of principle. We have shown that over the range of frequencies tested, the MEMS-μR can measure loss moduli ranging from 100 Pa to 6000 Pa using viscous standards of 2 Pa s and 10 Pa s. We conclude that the MEMS-μR can measure viscosities ranging from 1 Pa s (measured from 100 rad s^{-1} to 3000 rad s^{-1}) to 100 Pa s (ranging from 1 rad s^{-1} to 60 rad s^{-1}) which would give dynamically identical results to the modulus range the device has proven capable of measuring.

Viscoelastic thin film

The MEMS-μR was next tested with solid viscoelastic films, where $k_\sigma \equiv 0$. The moduli of PDMS can be varied by several orders of magnitude by adjusting the concentration of the cross-linking agent. At the lowest concentration of cross-linker used in this study, 1% by mass, PDMS resides in a viscoelastic regime close to the gel point.[38] PDMS samples of a similar composition to the ones used in this study have displayed a range of moduli values in the literature with variability of approximately ±10% of the modulus for a given experiment and batch to batch variability as high as 25%.[12,13,39–43] Reported values of elastic modulus for fully cured 3% PDMS have varied by a factor of approximately 1.6.[40,42,43] Furthermore, PDMS elastic moduli are also sensitive to curing conditions with moduli being affected by a factor of 4 based on curing time or temperature.[39,43] Therefore, although the fabrication of the PDMS thin films was done using identical procedures, we expect a degree of variability in the PDMS mechanical properties. We did not independently measure the modulus of our films because no technique suitable for 5 μm films was available.

The ability of the MEMS-μR to measure viscous and elastic moduli consistently was evaluated by testing 1% PDMS thin

Fig. 5 (a) Comparison of the physical model predicted (line) normalized amplitude, X, to observed experimental (symbols) results for 2 Pa s oil. (b) Strain on 2 Pa s oil for the same amplitudes. (c) Comparison of physical model predicted phase angle to observed experimental results for 2 Pa s oil. Phase angle experimental results fall within uncertainty of values predicted by the model.

agreement over the range of frequencies tested (Fig. 5c). These results are typical for both the viscous fluids tested. Using the phase angle and normalized amplitude from all the viscous oil experiments, the measured viscosity for the tested frequencies orbit the known values for the test fluids and are frequency independent (Fig. 6). The uncertainties on the data points were obtained by propagation of error. Starting with the uncertainty of coefficients from curves fitted to experimental data, the uncertainty was propagated through eqn (8) and (9). We do not report values for the lowest frequencies tested, because the capillary number is smaller than 0.1 at these frequencies. For these frequencies, the resulting extracted values of viscosity were 1 to 3 orders of magnitude larger than expected.

Up to approximately 100 rad s^{-1}, the uncertainty is a large percentage of the measured value, decreasing down to approximately 0.5% of the measured value at high frequencies. The
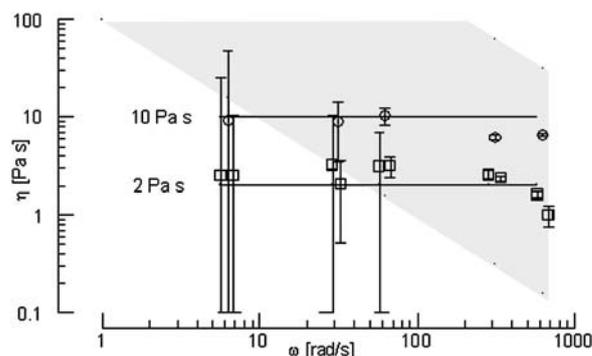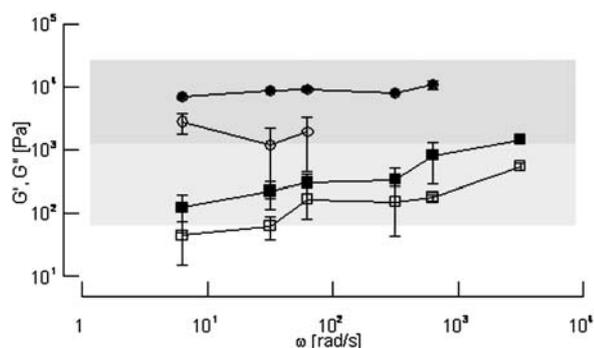
Fig. 7 (a) Storage modulus, G', in filled symbols and loss modulus, G'', in open symbols for (□) 1% PDMS and (○) 3% PDMS. Loss moduli for the 2 highest frequencies of the 3% PDMS decrease in value and increase in uncertainty due to the phase angle reaching its minimum resolution, and are removed from the graph. Darker shaded area represents theoretical measurement window for 3% data; entire shaded area represents theoretical measurement window for 1% data.

films on 4 MEMS-μR (Fig. 7). The deviation for the averaged moduli was 45%. The MEMS-μR average moduli are smaller by a factor of approximately four in comparison to reported values for bulk samples.[38] The 1% PDMS is close to the gel point, so small changes in concentrations could result in the observed deviations.[38] We also note that curing kinetics of poured bulk samples and spun thin films could be affected by the manner of fabrication, causing thin films to cure at different rates and resulting in the smaller observed moduli.[44] It is also possible that microstructural heterogeneity could be a factor in the lower than expected moduli. For similar PDMS systems, thin films with interfaces have displayed depth dependent heterogeneity that has reduced the rate of cross-linking.[45,46] In scarcely cross-linked PDMS films lower than expected moduli have been observed and theorized to be the result of planar microstructural heterogeneity.[47–49]

The storage modulus for the 3% PDMS obtained with the MEMS-μR (Fig. 7) is at the low end of reported values in literature.[40,42,43,50] The MEMS-μR storage moduli also correspond to the low end of measurements done on bulk samples of the same material (storage moduli of (11 ± 2) kPa to (78 ± 14) kPa, assuming a Poissons' ratio of 0.5 [51] using dynamic mechanical analysis with TA RSA 3). The 3% PDMS is a viscoelastic solid and the storage modulus does not vary considerably with frequency. These results are consistent with published frequency-dependent data.[38]

Both storage and loss moduli increase with cross-linker concentration, which is consistent with reported results.[38] These increases are well outside the uncertainty in the measurements. The less cross-linked films display a greater degree of dependence on frequency qualitatively, which is also consistent with published results and with proximity to the gel point.[38] There are not many published results on the behavior for this particular PDMS with cross-linker concentrations less than 3% by mass; nonetheless, the general frequency-dependent behavior for the PDMS films tested is consistent with published results and behavior of slightly gelled viscoelastic solid thin films.

In fully cross-linked PDMS spun films, a thickness dependent storage modulus has been reported with a transition from bulk

properties to thickness dependent properties at 200 μm.[44] The increased moduli at low thickness are due to high spin speeds causing high shear forces that reorder and stretch the random coil polymer chains. When the material is cross-linked, the stretched chains are fixed in that state, resulting in increased elastic moduli.[44] Although the films in this study are not fully cross-linked, the high spin speeds and fast cure times create similar effects in PDMS films 1 μm to 10 μm thick. Using the MEMS-μR, we can observe this phenomenon (Fig. 8).

At the lowest frequencies tested, the storage modulus for the thinner film is approximately 14 times greater than that of the film twice as thick. Although there is variability in PDMS properties, this is well above any variation reported in literature and the uncertainty of the measurements themselves so it is likely attributable to thin film stiffening. As the testing frequency increases, the thinner film continues to be stiffer, but the ratio between the moduli decreases slowly to 4. We observe that the viscous modulus also displays some increase with decreasing film thickness/increasing spin speed, but here the uncertainty of the measurement makes any definitive statement difficult. Unlike other experimental methods,[4,5,52] the MEMS-μR has the capability to monitor the effects of material reordering on both storage and loss modulus over a range of frequencies with a single measurement.
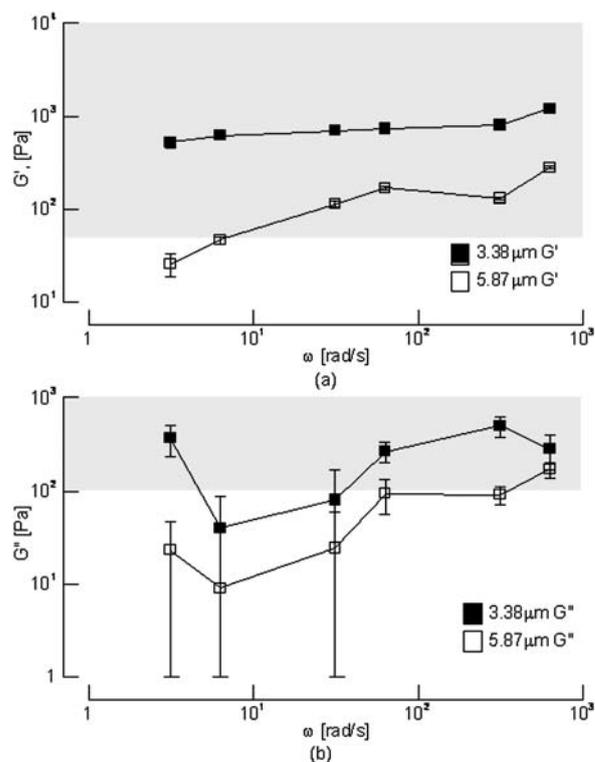

Fig. 8 (a) Storage modulus, G', 1% PDMS films with thicknesses of (3.38 ± 0.17) μm (■) and (5.87 ± 0.14) μm (□). (b) Loss modulus, G'', 1% PDMS films with thicknesses of (3.38 ± 0.17) μm (■) and (5.87 ± 0.14) μm (□). Shaded areas represent theoretical measurement windows.

Conclusion

The MEMS-µR allows us to measure both the viscosity/loss modulus and storage modulus for small volumes of materials, down to approximately 5 nL or less, with levels of confinement on the order of 1 µm. Through analysis of the stage motion and use of a physical model of the system dynamics, we characterize materials ranging from viscous fluids to viscoelastic thin films from 3 rad s^{-1} to 3000 rad s^{-1} and measuring moduli up to 10 kPa. Unlike other techniques, the MEMS-µR confines a material down to a few microns and shears the entire microstructure, measuring frequency-dependent response of storage and loss modulus, which creates a more complete picture of the material.

This first generation device has been able to characterize materials to an acceptable level of uncertainty and has shown its ability to distinguish moduli based on material composition and gap sizes, as long as moduli are distinct by approximately an order of magnitude. We believe that in the future the MEMS-µR can be redesigned to improve its accuracy, consistency and ease of use. Furthermore, redesigning the device and using a more accurate measurement of the sub-micron displacement of the stage will also give more consistent and accurate results when dealing with viscoelastic materials. In the future, the MEMS-µR should prove to be an effective additional tool for microrheology studies on a large array of materials.

References

1 R. G. Larson, *The Structure and Rheology of Complex Fluids*, Oxford University Press, New York, 1999.
2 T. A. Waigh, *Rep. Prog. Phys.*, 2005, **68**, 685–742.
3 C. J. Pipe and G. H. McKinley, *Mech. Res. Commun.*, 2009, **36**, 110–120.
4 C. Clasen and G. H. McKinley, *J. Non-Newtonian Fluid Mech.*, 2004, **124**, 1–10.
5 C. Clasen, B. P. Gearing and G. H. McKinley, *J. Rheol. (N. Y.)*, 2006, **50**, 883–905.
6 A. Mukhopadhyay and S. Granick, *Curr. Opin. Colloid Interface Sci.*, 2001, **6**, 423–429.
7 M. R. VanLandingham, J. S. Villarrubia, W. F. Guthrie and G. F. Meyers, *Macromol. Symp.*, 2001, **167**, 15–43.
8 J. M. Kranenburg, C. A. Tweedie, K. J. van Vliet and U. S. Schubert, *Adv. Mater.*, 2009, **21**, 3551–3561.
9 D. Moon, A. J. Bur and K. B. Migler, *J. Rheol. (N. Y.)*, 2008, **52**, 1131–1142.
10 M. S. N. Oliveira, M. A. Alves, F. T. Pinho and G. H. McKinley, *Exp. Fluids*, 2007, **43**, 437–451.
11 K. Kang, L. J. Lee and K. W. Koelling, *Exp. Fluids*, 2005, **38**, 222–232.
12 C. M. Stafford, C. Harrison, K. L. Beers, A. Karim, E. J. Amis, M. R. Vanlandingham, H. C. Kim, W. Volksen, R. D. Miller and E. E. Simonyi, *Nat. Mater.*, 2004, **3**, 545–550.
13 E. A. Wilder, S. Guo, S. Lin-Gibson, M. J. Fasolka and C. M. Stafford, *Macromolecules*, 2006, **39**, 4138–4143.
14 H. X. Mei, R. Huang, J. Y. Chung, C. M. Stafford and H. H. Yu, *Appl. Phys. Lett.*, 2007, **90**, 151902.
15 R. Huang, C. M. Stafford and B. D. Vogt, *J. Aerosp. Eng.*, 2007, **20**, 38–44.
16 C. C. White, M. R. Vanlandingham, P. L. Drzal, N. K. Chang and S. H. Chang, *J. Polym. Sci., Part B: Polym. Phys.*, 2005, **43**, 1812–1824.
17 P. M. Johnson and C. M. Stafford, *Rev. Sci. Instrum.*, 2009, **80**, 103904.
18 D. Tranchida, Z. Kiflie, S. Acierno and S. Piccarolo, *Meas. Sci. Technol.*, 2009, **20**, 095702.
19 P. M. McGuiggan and D. J. Yarusso, *J. Mater. Res.*, 2004, **19**, 387–395.
20 T. Gisler and D. A. Weitz, *Curr. Opin. Colloid Interface Sci.*, 1998, **3**, 586–592.
21 T. G. Mason and D. A. Weitz, *Phys. Rev. Lett.*, 1995, **74**, 1250–1253.
22 T. G. Mason, K. Ganesan, J. H. vanZanten, D. Wirtz and S. C. Kuo, *Phys. Rev. Lett.*, 1997, **79**, 3282–3285.
23 A. R. Bausch, W. Moller and E. Sackmann, *Biophys. J.*, 1999, **76**, 573–579.
24 A. Ashkin, *Proc. Natl. Acad. Sci. U. S. A.*, 1997, **94**, 4853–4860.
25 F. H. C. Crick and A. F. W. Hughes, *Exp. Cell Res.*, 1950, **1**, 37–80.
26 H. Matsuoka, S. Matsumoto and S. Fukui, *Microsyst. Technol.*, 2005, **11**, 1132–1137.
27 D. Cheneler, M. C. L. Ward, M. J. Adams and Z. B. Zhang, *Sens. Actuators, B*, 2008, **130**, 701–706.
28 J. J. Crassous, R. Regisser, M. Ballauff and N. Willenbacher, *J. Rheol. (N. Y.)*, 2005, **49**, 851–863.
29 L. Que, J. S. Park and Y. B. Gianchandani, *J. Microelectromech. Syst.*, 2001, **10**, 247–254.
30 S. Bergna, J. J. Gorman and N. G. Dagalakis, in *Micro-Electro-Mechanical Systems-2005*, Amer. Soc. Mechanical Engineers, New York, 2005, pp. 561–568.
31 J. J. Gorman, Y. S. Kim and N. G. Dagalakis, in *ASME International Mechanical Engineering Congress and Exposition*, Chicago, Illinois, 2006.
32 B. H. Kang, J. T. Y. Wen, N. G. Dagalakis and J. J. Gorman, *IEEE Trans. Rob.*, 2005, **21**, 1179–1185.
33 H. K. Wu, B. Huang and R. N. Zare, *Lab Chip*, 2005, **5**, 1393–1398.
34 A. L. Thangawng, R. S. Ruoff, M. A. Swartz and M. R. Glucksberg, *Biomed. Microdevices*, 2007, **9**, 587–595.
35 *Silicone Fluids: Stable, Inert Media*, Gelest, Inc., 2004.
36 B. Song and J. Sptinger, *J. Colloid Interface Sci.*, 1996, **184**, 77–91.
37 P. C. Painter and M. M. Coleman, *Fundamentals of Polymer Science: An Introductory Text*, CRC Press, Boca Raton, 1997.
38 J. Nase, A. Lindner and C. Creton, *Phys. Rev. Lett.*, 2008, **101**, 4.
39 J. N. Lee, X. Jiang, D. Ryan and G. M. Whitesides, *Langmuir*, 2004, **20**, 11684–11691.
40 X. Q. Brown, K. Ookawa and J. Y. Wong, *Biomaterials*, 2005, **26**, 3123–3129.
41 F. M. Sasoglu, A. J. Bohl and B. E. Layton, *J. Micromech. Microeng.*, 2007, **17**, 623–632.
42 F. Carrillo, S. Gupta, M. Balooch, S. J. Marshall, G. W. Marshall, L. Pruitt and C. M. Puttlitz, *J. Mater. Res.*, 2006, **21**, 535–537.
43 D. Fuard, T. Tzvetkova-Chevolleau, S. Decossas, P. Tracqui and P. Schiavone, *Microelectron. Eng.*, 2008, **85**, 1289–1293.
44 M. Liu, J. R. Sun, Y. Sun, C. Bock and Q. F. Chen, *J. Micromech. Microeng.*, 2009, **19**, 4.
45 T. R. E. Simpson, B. Parbhoo and J. L. Keddie, *Polymer*, 2003, **44**, 4829–4838.
46 T. R. E. Simpson, Z. Tabatabaian, C. Jeynes, B. Parbhoo and J. L. Keddie, *J. Polym. Sci., Part A: Polym. Chem.*, 2004, **42**, 1421–1431.
47 H. Takahashi, Y. Ishimuro and H. Watanabe, *Nihon Reoroji Gakkaishi*, 2006, **34**, 135–145.
48 H. Takahashi, Y. Ishimuro and H. Watanabe, *Nihon Reoroji Gakkaishi*, 2007, **35**, 191–198.
49 H. Takahashi, Y. Ishimuro and H. Watanabe, *Nihon Reoroji Gakkaishi*, 2009, **37**, 159–166.
50 Q. T. Nguyen, Z. Bendjama, R. Clement and Z. H. Ping, *Phys. Chem. Chem. Phys.*, 1999, **1**, 2761–2766.
51 *Polymer Handbook*, eds. J. Brandrup, H. Immergut and W. McDowell, Wiley, New York, 1975.
52 G. A. Davies and J. R. Stokes, *J. Non-Newtonian Fluid Mech.*, 2008, **148**, 73–87.